OPTIMAL ERROR ESTIMATE OF A DISCONTINUOUS GALERKIN METHOD FOR ONE-DIMENSIONAL LINEAR HYPERBOLIC EQUATION WITH DEGENERATE POINTS MOVING ALONG SPACE-TIME CURVES

YUAN XU*, XIONG MENG†, CHI-WANG SHU‡, AND QIANG ZHANG§

Abstract. In this paper we consider a discontinuous Galerkin method with purely upwind numerical flux to solve one-dimensional linear variable-coefficient hyperbolic equation, where the flow speed has different positive and negative signs when passing through the degenerate points. Our purpose is to give a rigorous proof of the optimal L^2-norm error estimate when the degenerate points move along smooth curves depending on both space and time. The main difficulty is how to deal with the signs' change of the flow speed regarding time. To this end, we propose a novel analysis framework with the help of a time-dependent projection based on the hybrid application of Gauss–Radau projections. First of all, we give a mesh-dependent subdivision of the computational domain and elaborately determine the space-time distribution of troubled locations, in which the type of Gauss–Radau projections suddenly switch with respect to the time variable. Then, we propose a union of bilinear forms (UBFs) with jump conditions to reflect the jumps along the time direction on troubled locations, for which a sharp boundedness concerning the accumulation of all involved jumps is proved. Finally, the optimal convergence order is derived by using the approximation properties of the time-dependent projection and the sharp boundedness for the UBFs. Numerical experiments are also given to validate the optimal order of accuracy.

Keywords. discontinuous Galerkin method, optimal error estimate, linear hyperbolic equation, degenerate point, space-time curve.

Mathematics Subject Classification (2020). 65M12; 65M15

1. Introduction.

In this paper, we concentrate on optimal error estimates of discontinuous Galerkin (DG) method for solving one-dimensional linear variable-coefficient hyperbolic equation with the flow speed of positive and negative signs. For the case that degenerate points (with zero flow speed) move along space-time curves, the standard analysis technique only derives a quasi-optimal L^2-norm error estimate with a half order reduction. To present a rigorous proof of optimal error estimates, we have to address the issues resulting from the sign distribution of the flow speed. For this purpose, we shall propose in this paper an analysis framework based on a novel application of Gauss–Radau (GR) projections, where a well-chosen mesh-dependent subdivision of the computational domain plays a vital role.

The DG method is one of the popular methods to solve hyperbolic equations by utilizing discontinuous finite element (piecewise polynomials) spaces. This method was firstly introduced by Reed and Hill [21] for a steady-state linear neutron transport equation, and then developed by Cockburn et al. [10–14] to solve time-dependent nonlinear conservation laws. Coupled with an efficient time marching techniques, for example, the strong stability preserving Runge–Kutta method, this method has been widely applied to computational fluid dynamics. Numerical experiments show that the DG method exhibits strong stability and high accuracy, with the ability to sharply capture shocks. For more details, please refer to the review papers [8,9] and the references therein.

Even though plenty of theoretical analysis on DG methods have been given in the literature, there are still gaps between theory and numerical results. For instance, an interesting and important topic that will be discussed in this paper is the optimal error estimate of the DG methods when

*School of Mathematical Sciences, Nanjing Normal University, Nanjing 210023, Jiangsu Province, China. E-mail: yuanxu@njnu.edu.cn. Research was supported by NSFC grants 12301513, 12071214, Natural Science Foundation of Jiangsu Province grant BK20230374 and Natural Science Foundation of Jiangsu Higher Education Institutions of China grant 23KJB110019.

†School of Mathematics, Harbin Institute of Technology, Harbin 150001, Heilongjiang Province, China. E-mail: xiongmeng@hit.edu.cn. The research of this author was supported by NSFC grants 12371365, 11971132, Natural Science Foundation of Heilongjiang Province grant YQ2021A002, and the Fundamental Research Funds for the Central Universities grant HIT.OCEF.2022031.

‡Division of Applied Mathematics, Brown University, Providence, RI 02912, USA. E-mail: chi-wang_shu@brown.edu. The author was supported by NSF grant DMS-2309249.

§Corresponding author. School of Mathematics, Nanjing University, Nanjing 210093, Jiangsu Province, China. E-mail: qzh@nju.edu.cn. Research was supported by NSFC grant 12071214.

degenerate points move left and right such that the relevant trajectories are no longer limited to the vertical or horizontal lines in the space-time domain. Indeed, this phenomenon about the flow speed occurs in many practical problems. For example, this phenomenon includes: 1) the shallow water equations [24] with rapidly moving interfaces between wet and dry areas such as dam breaks, flood waves and run-up phenomena over shores; 2) the compressible Euler equations with a source term [29], arising from gravity, chemical reaction or radiative cooling; 3) Vlasov–Poisson equations [23] with the changed direction of the electric field. Although the optimal convergence order for the above examples can be numerically observed for smooth solutions, how to rigorously derive optimal error estimate has not been carefully and systematically studied till now.

To better understand our research purpose of this paper, we would like to recall some existing works on error estimates of the DG methods, in which the involved techniques and ideas are helpful for us to achieve the aim. As is well known, the quasi-optimal convergence order $k + 1/2$ can be easily proved by the local L^2-projection no matter whether the sign of the flow speed changes or not; see [16] for example. Here k is the degree of piecewise polynomials used in the DG method. As an important topic in theoretical analysis, how to derive optimal error estimates has been studied by many researchers. For the linear constant-coefficient hyperbolic equation in one dimension, the optimal convergence order $k + 1$ was proved in [9] for the DG method with the purely upwind numerical fluxes. The key ingredient of the proof is the application of the GR projection, which is a particular projection depending on the sign of flow speed on each element. In [20], the above work is successfully extended to the DG method with the upwind-biased numerical fluxes, with the help of the generalized GR projection. As an application of the above projections, the optimal error estimate is easily obtained for linear variable-coefficient hyperbolic equations or nonlinear conservation laws, if the flow speed does not change signs (meaning either positive or negative) on the computational domain. However, some additional theoretical difficulties emerge when the flow speed passes through zero, and only a few optimal error estimates are available for special cases till now. For example, one-dimensional linear problem was studied in [17], where the flow speed depends solely on the spatial variable. Two-dimensional linear problem was also investigated in [19], where each component of the flow speed depends only on the spatial variable in the same direction. For one dimensional nonlinear conservation laws with sufficiently smooth exact solution, the optimal error estimate of the DG method was obtained for the generalized local Lax–Friedrichs flux [18], the upwind flux [27, 28], and a class of widely-used numerical fluxes [1]. As an important technical tool, the carefully-designed projections in the aforementioned works are all continuously differentiable (or unchanged in most cases) with respect to the time variable.

In summary, the optimal error estimate available in the references is mainly restricted to the following two simple cases. One is that the position of degenerate points (if exist) is independent of time, and the other is that the sign of flow speed does not cross zero. We remark that this limitation also exists for other numerical methods, e.g., finite volume method [3, 4] and spectral volume method [25]. In this paper, we would like to overcome this limitation and explore a rigorous proof of optimal error estimate for DG methods. As the first step on this issue, we would like to start from the DG method with the purely upwind numerical flux to solve one-dimensional linear hyperbolic equation, of which the flow speed has different signs and a finite number of trajectories of degenerate points with representative structures. For the case that each trajectory is a space-time curve, it is challenging to strictly prove the optimal error estimate. To our best knowledge, this paper is the first work to provide a distinctive strategy and a solid analysis on this topic.

The techniques proposed in this paper can be clearly explained by the simplest case that only one trajectory of degenerate points smoothly moves leftward (or rightward) and the flow speed has different positive or negative signs to both sides of this trajectory. Such flow field leads to an intrinsic difficulty in constructing and analyzing the time-dependent projection based on the application of two types of GR projections. That is, for any given element and time, the designed projection is locally defined to be a GR projection on this element and the detailed type of GR projection depends heavily on the location sign, which can be roughly understood as the positive or

negative sign of the flow speed at this location. In this paper, the terminology *location* represents the Cartesian product of an element and a given time; see (4.1). Since the degenerate points move along space-time curves, the flow speed cannot keep a fixed sign on each rectangular column (the Cartesian product of an element and the whole time interval) intersected by the trajectory. In other words, the location sign will inevitably encounter a sudden change at some moments. As a direct consequence, the type of GR projections is subject to sudden changes at some locations, and the time-dependent projection error for the exact solution is double-valued and thus discontinuous at the relevant time. In this paper, such mesh-dependent moments and locations are called troubled moments and troubled locations, respectively. It is worth pointing out that the analytical difficulty arises from Proposition 4.1 that the total number of troubled moments is of order $\mathcal{O}(h^{-1})$, where h is the size of spatial mesh. This property may cause the loss of convergence order if we do not carry out a careful analysis. Even with the help of GR projections, excessively rough estimates may not allow us to achieve the quasi-optimal order $k+1/2$, which, however, can be easily obtained by the simple L^2 projection without taking into account the distribution of flow speed.

Motivated by the above discussions, we have to build in this paper a novel framework coupled with some new techniques to achieve the optimal error estimate. Basically, the essential change in our proof line results from the new explanation on the error decomposition $\mathcal{E}(t)=\xi(t)-\eta(t)$; see (4.22). Here $\mathcal{E}$ is the numerical error, ξ is the error in the finite element space, and η is the projection error for the exact solution. Compared with the classical analysis, the main difference in this paper is that both ξ and η are allowed to be discontinuous at some times despite of the continuity of $\mathcal{E}$ with respect to time. This new explanation has been adopted in our previous work about the analysis on the RKDG methods with stage-dependent numerical fluxes; see [26] for more details.

Associated with the above new insight on the error decomposition, we have to address two fundamental issues. The first issue is the definition and control of η. As we have mentioned before, the time-dependent projection is a hybrid application of two types of GR projections, whose specific definition is uniquely determined by the location sign. In this paper, the location sign certainly originates from the subregion sign[1] if the location and the subregion comply with an inclusion relationship. Hence, the above task can be naturally transformed into a geometric problem on how to suitably define a mesh-dependent subdivision of the computational domain such that the control of η and its jumps' accumulation are all in optimal order.

The second issue is the optimal estimate to ξ. Analogous to the traditional treatment, this issue also starts from the error equation, which, however, is not easy to accomplish. Due to the discontinuity of both η and ξ, the error equation in the traditional sense only holds in every small time interval separated by the troubled moments. Owing to the continuity of $\mathcal{E}$, the error ξ satisfies the jump condition at each troubled moment, which is explicitly shown by the jumps of projection errors along the time direction on troubled locations. We remark that all of these formulas involved constitute a new discrete system, which has a slightly different form to the original DG method. This is the main improvement in our analysis framework. To avoid the order reduction theoretically, we have to set up a double-optimality concerning the time accumulation of those jumps of projection errors in the sense that not only the accumulation itself is of optimal order but also the amplification factor of the accumulation is sharply bounded.

We would like to emphasize that the aforementioned issues can be well addressed by a mesh-dependent subdivision of the computational domain, which matches the trajectory of degenerate points with the discontinuous feature of the time-dependent projection. To this end, we need to explore a delicate way to partition the computational domain into the left and right subregions with opposite subregions signs. This purpose can be implemented in the following three steps. First, we find the transition subregion that includes all locations intersecting the trajectory of degenerate points, and divide the computational domain into three subregions. Then, we combine two adjacent subregions that have the same subregion sign. Since the transition subregion has two possible

[1] Throughout this paper, the location and the subregion are defaulted to closed sets in the computational domain, with dimension number of 1 and 2, respectively.

assignments on the subregion sign, we have two choices on the subdivision of two subregions with different signs. Finally, we pick up the desired mesh-dependent subdivision from these two choices, which identifies an essential subregion with the staircase-shape outflow boundary such that both the hyperbolic equation and the DG method with the purely upwind numerical flux can be independently solved by those data given there.

For the sake of easy reading, some more detailed procedures are explained as follows. In Subsection 4.1, we define a mesh-dependent subdivision to partition the computational domain into the left and right subregions with opposite subregions signs. In Subsection 4.2, we present a union of bilinear forms (UBFs) with jump conditions, i.e., a new discrete system corresponding to the error equation about ξ. By fully utilizing the geometric structure of the essential subregion and the locally nonzero property of jump functions on each troubled location, we are able to establish a sharp boundedness for the UBFs. That is, the time accumulation of all jump functions $\sum_{1\le n\le m_h}\|g^n\|^2_{L^2(\mathrm{TE}(n))}$ possesses the coefficient of order $\mathcal{O}(1)$ instead of $m_h=\mathcal{O}(h^{-1})$; see (4.7) in Lemma 4.1, and (4.18) in Remark 4.2 below. This result is the crucial step to achieve the optimal error estimate, where the subtle applications of Gronwall-type inequalities also play an important role. In Subsection 4.3, after determining the time-dependent projections, we use a novel error decomposition to obtain the optimal error estimate, by combining the sharp boundedness for the UBFs, the approximation properties of projections as well as the estimate of the exact solution.

The rest of this paper is organized as follows. In Section 2, we present the definition of the DG method and the optimal error estimate, followed by some comments on the proof of Theorem 2.1. Preliminaries including Gronwall-type inequalities, GR projections and inverse inequalities are given in Section 3. As the main body of this paper, Section 4 provides the proof for a simple case where degenerate points smoothly moves only along a single trajectory, in which the concepts concerning the mesh-dependent subdivision, the troubled locations, and the sharp boundedness of the UBFs are clearly illustrated. In Section 5, we extend the proof from a single trajectory to multiple trajectories, where the technicalities are updated to address some extra difficulties. In Section 6, numerical experiments are displayed to demonstrate the optimal convergence order. Concluding remarks are provided in Section 7.

2. The DG method and the main result. The model problem considered in this paper is the purely initial value problem of a linear variable-coefficient hyperbolic equation

$$\begin{aligned} U_t(x,t)+\Big[\beta(x,t)U(x,t)\Big]_x&=f(x,t),\quad t\in(0,T],\quad x\in\mathbb{R}=(-\infty,+\infty),\\ U(x,0)&=U_0(x),\quad x\in\mathbb{R}, \end{aligned}\tag{2.1}$$

where $T>0$ is the final time and $U_0(x)$ is the initial condition. For simplicity, we would like in this paper to assume that both the flow speed $\beta(x,t)$ and the source term $f(x,t)$ are sufficiently smooth (at least continuous) on the closed computational domain $\Omega=\mathbb{R}\times[0,T]$. Considering our interest in this paper, we further assume that $\beta(x,t)$ has different signs. More discussions will be given in Subsections 2.2 and 2.3.

2.1. Semidiscrete DG method. Denote by $\mathbb{Z}$ the set of integers. Let $I_h=\{I_j\}_{j\in\mathbb{Z}}$ form the quasi-uniform mesh of $\mathbb{R}$, where each closed element $I_j=[x_{j-1/2},x_{j+1/2}]$ has the length $h_j=x_{j+1/2}-x_{j-1/2}$. Denoting by $h=\max_{j\in\mathbb{Z}}h_j\le 1$ the mesh size, the discontinuous finite element space is defined as usual, namely

$$V_h=\{\,v\in L^2(\mathbb{R}):v|_{I_j}\in\mathcal{P}^k(I_j),\,\forall\, j\in\mathbb{Z}\,\},\tag{2.2}$$

where $\mathcal{P}^k(I_j)$ is the space of polynomials on I_j of degree at most $k\ge 0$. The jump at element endpoint is denoted by $[\![v]\!]=v^+-v^-$, where v^- and v^+ respectively denote the left and right limits of v, as usual.

For the convenience of notations, we would like in this paper to denote

$$\Big(w,v\Big)_{I_h}=\sum_{j\in\mathbb{Z}}\int_{I_j}wv\,\mathrm{d}x,\quad \Big\langle w^{\mathrm{b}},v^{\mathrm{b}}\Big\rangle_{\Gamma_h}=\sum_{j\in\mathbb{Z}}w^{\mathrm{b}}_{j+\frac12}v^{\mathrm{b}}_{j+\frac12},$$

where the superscript b is used to emphasize that the involved function is single-valued on the set of element endpoints, denoted by $\Gamma_h=\{x_{j+1/2}\}_{j\in\mathbb{Z}}$. Here and below, the space and/or time argument of a function will be dropped for convenience, if there is no confusion.

The DG method considered in this paper is defined as follows: find the map $u(t)\colon[0,T]\to V_h$, such that it satisfies the initial condition $u(x,0)=u_0(x)\in V_h$ and the weak form

$$\Big(u_t,v\Big)_{I_h}=\mathcal{H}(t;u,v)+\Big(f,v\Big)_{I_h},\quad \forall\, v\in V_h, \tag{2.3}$$

for any $t\in(0,T]$. Here the DG spatial discretization operator is given in the form

$$\mathcal{H}(t;u,v)=\Big(\beta(t)u(t),v_x\Big)_{I_h}+\Big\langle\widehat{\beta(t)u(t)},[\![v]\!]\Big\rangle_{\Gamma_h}, \tag{2.4}$$

and the hat function is the numerical flux. In this paper the purely upwind numerical flux is adopted, namely

$$\widehat{\beta(t)u(t)}\Big|_{j+\frac12}=\beta_{j+\frac12}(t)\Big[A_{j+\frac12}u^-_{j+\frac12}(t)+(1-A_{j+\frac12})u^+_{j+\frac12}(t)\Big], \tag{2.5}$$

with $\beta_{j+1/2}(t)=\beta(x_{j+1/2},t)$ and $A_{j+1/2}=\operatorname{sgn}\beta_{j+1/2}(t)$.

The initial solution $u_0(x)$ can be taken as any suitable approximation of $U_0(x)$. To ensure the optimal L^2 norm error estimate of this method, we demand

$$\|U_0-u_0\|_{L^2(\mathbb{R})}\le Ch^{k+1}, \tag{2.6}$$

where C is a positive constant independent of h. For example, $u_0(x)$ can be defined as the local L^2-projection of $U_0(x)$, which is the unique function in V_h such that $(u_0,v)_{I_h}=(U_0,v)_{I_h}$ holds for any $v\in V_h$. Till now we have completed the definition of the DG method for the model problem (2.1).

2.2. Regularity. The standard notations and norms for Sobolev space are used throughout this paper. For any given positive integer a and space domain D, we use $C(H^a(D))$ to denote the space-time Sobolev space of which the $H^a(D)$ norm is continuous and hence bounded on $[0,T]$.

In order to carry out error estimates, we would like to assume that the exact solution $U(x,t)$ is sufficiently smooth. For example, we assume in this paper that the known data of (2.1) satisfy

$$\beta\in C(H^{k+3}(\mathbb{R})),\quad \beta_t\in C(H^{k+2}(\mathbb{R})),\quad f\in C(H^{k+2}(\mathbb{R})). \tag{2.7}$$

These conditions ensure the regularity assumption of the exact solution [2, Chapter 2]

$$U(x,t)\in C(H^{k+2}(\mathbb{R})),\quad U_t(x,t)\in C(H^{k+1}(\mathbb{R})), \tag{2.8}$$

provided that the initial solution satisfies $U_0\in H^{k+2}(\mathbb{R})$. Note that these conclusions hold true no matter whether degenerate points exist or not.

For the numerical solution, we have the following proposition.

PROPOSITION 2.1. *If (2.7) holds, for any h, the map $u(t)\colon[0,T]\to V_h$ exists uniquely and is continuously differentiable.*

Proof. This proposition can be proved by the Cauchy-Lipschitz-Picard theorem in Banach space [5, Theorem 7.3]. The detailed proof is omitted here. ∎

By the above discussion we know that the error $\mathcal{E}(t)=u(t)-U(t)\colon[0,T]\to L^2(\mathbb{R})$ is continuously differentiable with respect to t. This is a key point of the error estimate. Further discussion will be given in Subsection 4.3.2.

2.3. Optimal error estimate. The proof of the optimal error estimate depends on the sign distribution of the flow speed. In this paper, we would like to make some assumptions as follows.

(A1) There are a finite number of continuously differentiable trajectories of degenerate points, with different survival times between appearance and disappearance. These trajectories are allowed to change the moving direction (or the monotonicity of time) and intersect with each other up to a limited number of times. Without counting the repeated time, all related moments can be ordered in a finite number of sequence

$$0 = t^{(0)} < t^{(1)} < t^{(2)} < \cdots < t^{(M-1)} < t^{(M)} = T. \tag{2.9}$$

(A2) On each time interval given by (2.9), it is acceptable to assume that the trajectories from left to right can be represented by monotone and continuously differentiable functions

$$x = \ell_i(t), \quad i = 1, 2, \ldots, s, \tag{2.10}$$

where s is a positive integer independent of h. Each adjacent distance between two adjoining trajectories, denoted by a nonnegative function

$$d_i(t) = \ell_{i+1}(t) - \ell_i(t), \quad i = 1, \ldots, s-1, \tag{2.11}$$

has a limited number of times such that the monotonicity is changed. Further, we assume that the positive and negative signs of the flow speed are alternatively distributed on both sides of each trajectory.

A descriptive illustration for this assumption is plotted in Figure 1, where the left trajectory changes the moving direction twice and the others intersect to each other once. The dash line connecting D and E is an example to mark the moment when the adjacent distance locally achieves the maximum.

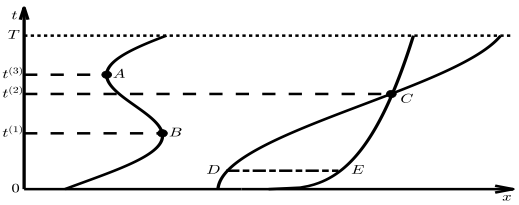

FIG. 1. *Example of Assumption (A).*

REMARK 2.1. *The above assumption excludes the trivial case that the flow speed does not cross zero, since the optimal error estimate is easily obtained by using a same type of GR projection.*

For the convenience of notations, throughout this paper we use a generic symbol C (maybe with subscripts) to denote a positive constant independent of h. They may have different values in each occurrence.

We are now ready to state the main result of the DG method solving linear hyperbolic equations with degenerate points satisfying Assumption (A).

THEOREM 2.1. *Let U be the exact solution of the model problem (2.1) satisfying (2.7) and (2.8), and u be the DG solution of (2.3) satisfying (2.6). Then, we have the optimal error estimate*

$$\|u(T) - U(T)\|_{L^2(\mathbb{R})} \le Ch^{k+1} \tag{2.12}$$

under Assumption (A). Here the bounding constant $C > 0$ is independent of h.

Some comments on the proof of this theorem are given below. Due to the finiteness of (2.9) and the continuity of $\mathcal{E}(t) = u(t) - U(t)$, Theorem 2.1 can be proved by inductively proving

$$\|\mathcal{E}(t^{(i)})\|_{L^2(\mathbb{R})} \le C_i h^{k+1}, \quad i = 0, 1, \ldots, M,$$

where the constant $C_i > 0$ is independent of h. For $i = 0$, it obviously holds due to (2.6). For $i > 0$, the proof is almost the same, if the time interval $[t^{(i-1)}, t^{(i)}]$ is denoted by $[0, T]$ for the convenience of notations. Hence, in what follows we just need to concentrate on how to strictly prove Theorem 2.1 under Assumption (A2).

REMARK 2.2. *The above proof strategy also works well for horizontal trajectories of degenerate points.*

To clearly show our analysis framework to achieve the above goal, we would like in Section 4 to present the rigorous proof of Theorem 2.1 for a single trajectory under the following assumptions:

(B1) The unique trajectory function, denoted by $x = x_\star(t)$ now, is continuously differentiable and strictly monotone (increasing or decreasing) on the time interval $[0, T]$;

(B2) The flow speed has different signs on both sides of the trajectory.

Some important concepts and techniques are also proposed and discussed there. The extension to multiple trajectories will be provided in Section 5.

REMARK 2.3. *Assumption (B) has removed an undistinguished case that degenerate points move along a vertical trajectory, since the optimal error estimate for this case has been obtained in some existing works, as mentioned in the introduction.*

3. Preliminaries.

Some preliminaries regarding Gronwall-type inequalities, GR projections and inverse inequalities are given in this section.

3.1. Gronwall-type inequalities.

Two types of Gronwall inequalities will be used in this paper. One is the classical version for continuous functions [15], and the other can be looked upon as an extension of the discrete version. The proofs are trivial and hence omitted here.

LEMMA 3.1. *Let $Z(t)$ and $F(t)$ be nonnegative and continuous functions. If there exists a constant $q > 0$ such that $\frac{\mathrm{d}}{\mathrm{d}t} Z(t) \le qZ(t) + F(t)$ holds for any $t \in (a, b]$, then we have*

$$Z(b) \le e^{q(b-a)} \Big(Z(a) + \int_a^b F(t)\,\mathrm{d}t \Big).$$

LEMMA 3.2. *Let $\{Z^n\}_{n=0}^N$, $\{G^n\}_{n=1}^N$ and $\{F^n\}_{n=0}^N$ be nonnegative sequences, where N is a positive integer. If there are two constants $\gamma \ge 1$ and $q > 0$ such that*

$$Z^{n+1} + G^{n+1} \le \gamma e^{q(t^{n+1} - t^n)} (Z^n + F^n), \quad 0 \le n \le N-1, \tag{3.1}$$

where $t^0 < t^1 < \cdots < t^N$, then we have

$$Z^N + \sum_{n=1}^{N} G^n \le \gamma^N e^{q(t^N - t^0)} \Big(Z^0 + \sum_{n=0}^{N-1} F^n \Big). \tag{3.2}$$

3.2. GR projection.

It is a widely-used tool in deriving optimal error estimate of DG methods, when purely upwind numerical fluxes are used. On each element there are two types of locally-defined GR projections associated with the exact collocation at a certain endpoint,

DEFINITION 3.1. *Let $w(x)$ be a given smooth function. For any $j \in \mathbb{Z}$, two GR projections on the element I_j, denoted by $\mathbb{G}_{j,\pm} w$, are respectively the unique function in $\mathcal{P}^k(I_j)$ such that*

$$\int_{I_j} \big(\mathbb{G}^{\perp}_{j,\pm} w \big) v \,\mathrm{d}x = 0 \quad \forall\, v \in \mathcal{P}^{k-1}(I_j), \quad \text{and} \quad \big(\mathbb{G}^{\perp}_{j,\pm} w \big)^{\mp}_{j \pm \frac{1}{2}} = 0, \tag{3.3}$$

where $\mathbb{G}^{\perp}_{j,\pm} w = w - \mathbb{G}_{j,\pm} w$ denotes the projection error of w. If $k = 0$, the first condition in (3.3) is not necessary.

As shown in [6, Lemma 3.3], both GR projections are well-defined and satisfy the approximation property

$$\|\mathbb{G}^{\perp}_{j,\pm}w\|_{L^2(I_j)} + h^{\frac{1}{2}}\|\mathbb{G}^{\perp}_{j,\pm}w\|_{L^2(\partial I_j)} \le Ch^{k+1}\|w\|_{H^{k+1}(I_j)}, \tag{3.4}$$

where the bounding constant $C > 0$ is independent of j, w and h. Here we use the notation for smooth function w as follows:

$$\|w\|_{L^2(I_j)} = \left(\int_{I_j} w^2\,\mathrm{d}x\right)^{\frac{1}{2}}, \quad \|w\|_{L^2(\partial I_j)} = \left[(w^+_{j-\frac{1}{2}})^2 + (w^-_{j+\frac{1}{2}})^2\right]^{\frac{1}{2}}.$$

3.3. Inverse inequalities. Some inverse inequalities will be used in this paper. That is, for any $j \in \mathbb{Z}$ and $v \in \mathcal{P}^k(I_j)$, there hold [7]

$$\|v_x\|_{L^2(I_j)} \le \mu h^{-1}\|v\|_{L^2(I_j)}, \quad \|v\|_{L^2(\partial I_j)} \le \mu h^{-\frac{1}{2}}\|v\|_{L^2(I_j)}, \tag{3.5}$$

where $\mu > 0$ is the inverse constant independent of j, v and h.

4. Proof of Theorem 2.1 for a single trajectory. In this section we present a novel analysis framework to rigorously obtain the optimal error estimate under Assumption (B). To do that, we start, in Subsection 4.1, by defining the mesh-dependent subdivision to determine the essential subregion and the troubled locations of this trajectory. Then, we move on to Subsection 4.2 by introducing the UBFs with a provable sharp boundedness for the time accumulation of jump functions. Finally, in Subsection 4.3, we identify the time-dependent projection and obtain optimal error estimates.

4.1. The mesh-dependent subdivision. In this subsection, we present our strategy on how to define a mesh-dependent subdivision of the computational domain, which is the foundation stone of our analysis.

4.1.1. Troubled moments and transition subregion. To capture the numerical effect of the moving of degenerate points, we need to make a distinction between the positive and negative signs for all locations

$$I_j(t) \equiv \{(x,t)\colon x \in I_j\}, \quad j \in \mathbb{Z}, \quad t \in [0,T]. \tag{4.1}$$

The crucial step to complete this task is to determine the *transition subregion*, which is made up of all locations intersecting the trajectory of degenerate points.

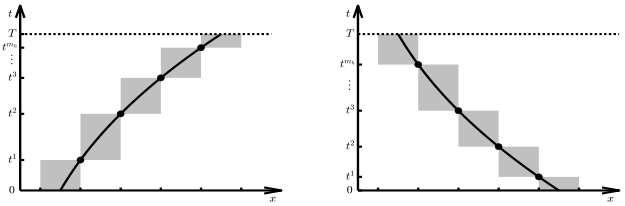

FIG. 2. *The transition subregion $\Omega_\star$ (shadow) along the trajectory of degenerate points.*

Below we give a detailed description on the concept of transition subregion by Figure 2. Since the considered trajectory $x_\star(t)\colon [0,T] \to \mathbb{R}$ is strictly monotone and continuously differentiable, as stated in Assumption (B1), there exist m_h *troubled moments*

$$0 < t^1 < t^2 < \cdots < t^{m_h} < T, \tag{4.2}$$

such that $x_\star(t^n)$ is precisely an element endpoint for $n = 1, 2, \ldots, m_h$. For the convenience of notations, we denote $t^0 = 0$ and $t^{m_h+1} = T$ in addition.

We remark that troubled moments result in the main difficulty of theoretical analysis in this paper, which is stated in the following proposition.

PROPOSITION 4.1. *Under Assumption (B1), the total number of troubled moments satisfies*

$$C_1 h^{-1} \leq m_h \leq C_2 h^{-1},$$

for sufficiently small h, where C_1 and C_2 are two positive constants independent of h.

Proof. Since $x_\star(T) - x_\star(0)$ is a nonzero number independent of h, due to Assumption (B1), the proof of this proposition is trivial by using the quasi-uniform property of I_h. ∎

For $n = 1, 2, \ldots, m_h$, there are the left and right elements sharing the element endpoint $x_\star(t^n)$. In this paper, we denote them by $I_{l(n)}$ and $I_{r(n)}$ respectively, with $r(n) = l(n)+1$. Now the transition subregion, denoted by $\Omega_\star$, can be explicitly formulated as follows. For the case that the degenerate points move rightward (namely the trajectory sign is positive), we have

$$\Omega_\star = \bigcup_{n=0}^{m_h} I_{r(n)} \times [t^n, t^{n+1}] = \bigcup_{n=1}^{m_h+1} I_{l(n)} \times [t^{n-1}, t^n], \tag{4.3}$$

with the supplementary notations $r(0) = l(1)$ and $l(m_h + 1) = r(m_h)$. We remark that $\{l(n) : 1 \leq n \leq m_h + 1\}$ and $\{r(n) : 0 \leq n \leq m_h\}$ are two increasing sequences between two integers, respectively. For the opposite case that the degenerate points move leftward (namely the trajectory sign is negative), the transition subregion can be similarly defined and hence omitted here.

There are two subregions beside the transition subregion $\Omega_\star$. The left and right subregions are denoted by Ω_{L} and Ω_{R}, respectively. That is, the computational domain is subdivided in the form $\Omega = \Omega_{\mathrm{L}} \cup \Omega_\star \cup \Omega_{\mathrm{R}}$, where the interior of the three subregions is not overlapping, and any location lies on either one of the three subregions or the common boundary of two adjacent subregions. Till now we complete the initial classification of locations.

4.1.2. Subregion sign and location sign. It is well known that the type of GR projection depends on the sign distribution of the flow speed on each location, which is quantified as the *location sign* in this paper.

To define the location sign for each location, we start from the discussion on the subregion sign for a subregion. The relevant conclusion is given as follows.

- If the flow speed has the same sign (positive or negative) in the interior of a subregion, then the subregion sign is naturally defined as this sign. As a conclusion, the subregion signs of Ω_{L} and Ω_{R} are unambiguous.
- If the flow speed has different signs in a subregion, the subregion sign can be defined as either positive or negative; see the transition subregion $\Omega_\star$ as an example.

The subregion sign is then used to define the location sign by the next definition.

DEFINITION 4.1. *For any location contained by a subregion, the location sign is inherited from the subregion sign of this subregion.*

This definition implies that the location sign may be double valued if the location simultaneously lies on two subregions (and hence the common boundary of them). As an important observation, two values of the local sign can be understood as the limits in different subregions.

4.1.3. Subdivision, essential subregion and troubled locations. We are now ready to define the desired subdivision by correctly determining the subregion sign of $\Omega_\star$ and combining adjacent subregions with the same sign.

This aim can be achieved by the following observation. Due to Assumption (B2), the subregion signs of Ω_{L} and Ω_{R} are opposite. No matter how we define the subregion sign for $\Omega_\star$, either Ω_{L} or

$\Omega_{\rm R}$ has the same subregion sign as that of $\Omega_\star$. After the combination of adjacent subregions with the same sign, we can get two extended subregions with opposite subregion signs. The crucial step in our analysis framework is to determine the *mesh-dependent subdivision* between two possible choices, such that the hyperbolic equation (2.1) forms a closed system on a certain extended subregion. Such extended subregion is named the *essential subregion* in this paper, since the exact solution of (2.1) can be uniquely and independently determined by the initial data and the source term involved there.

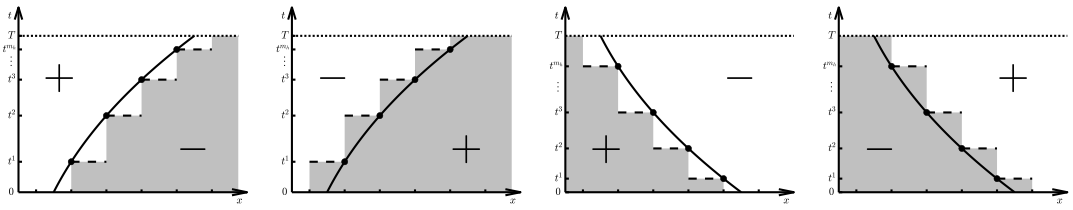

FIG. 3. *The essential subregion (shadow) and the troubled locations (dash lines) for four cases, where the flow speed has positive (+) and negative (−) sign beside the trajectory of degenerate points.*

Figure 3 describes all possible combinations of the trajectory sign and the sign distribution of the flow speed, where the essential subregion is marked by shadow. From these pictures, three equivalent principles to determine the subdivision are given below.

- The subregion sign of $\Omega_\star$ is defined as the trajectory sign.
- For the extended subregion whose interior does not contain the trajectory, the subregion sign is opposite to the trajectory sign.
- The common boundary of the extended subregions is the outflow boundary of one of them, which is just the essential subregion.

In these pictures, the dash line marks the *troubled location*, which is a special location standing on the common boundary of the essential subregion and the adjacent extended subregion.

Figure 3 shows that the troubled locations only occur at the troubled moments and have the double-valued location signs. For $n = 1, 2, \ldots, m_h$, we denote the troubled location by

$$\mathrm{TL}(n) = \mathrm{TE}(n) \times \{t^n\} = \{(x,t)\colon x \in \mathrm{TE}(n), t = t^n\},$$

where $\mathrm{TE}(n)$ is called the troubled element. Obviously, one can see $\mathrm{TE}(n) = I_{r(n)}$ if the flow speed is negative on the right (or left) of the positive (or negative) trajectory. For the other case, we have $\mathrm{TE}(n) = I_{l(n)}$. For convenience, the above notations can be extended to $n = m_h + 1$.

Let us make a detailed illustration of the essential subregion. Figure 3 also shows that this subregion is made up of a union of space-time stripes, namely

$$\Omega_{\star\star} = \bigcup_{n=1}^{m_h+1} \mathrm{TH}(n) \times [t^{n-1}, t^n], \tag{4.4}$$

where $\mathrm{TH}(n) = \{I_j\colon I_j(t^n) \subset \Omega_{\star\star}\}$ is the spatial half-line started from $\mathrm{TE}(n)$. Furthermore, we have the following propositions for the essential subregion:

(P1) As the outflow boundary of the essential subregions, each vertical boundary nearby the trajectory has a fixed sign of the flow speed. If the trajectory moves to the right (see the first two pictures of Figure 3), the flow speed is nonpositive; otherwise, the flow speed is nonnegative.

(P2) For $n = 1, 2, \ldots, m_h$, the troubled location $\mathrm{TL}(n)$ does not belong to the common boundary of two adjacent stripes. Furthermore, the interior of $\mathrm{TE}(n)$ and $\mathrm{TH}(n+1)$ are not overlapped and there holds the geometric structure relationship

$$\mathrm{TE}(n) \cup \mathrm{TH}(n+1) = \mathrm{TH}(n). \tag{4.5}$$

If we introduce supplementary notations $\mathrm{TH}(0) = \mathrm{TH}(1)$ and $\mathrm{TE}(0) = \emptyset$, this conclusion is also true for $n = 0$.

These properties will play important roles in the next subsection.

To end this subsection, we would like to emphasize again that the location sign for any location has been properly defined by the obtained subdivision and the relevant subregion signs, due to Definition 4.1.

4.2. A sharp boundedness for the UBFs. Associated with the obtained subdivision, we would like to introduce jump functions on troubled locations and define a union of bilinear forms (UBFs) with jump conditions as follows.

- Let $z_0(x) \in V_h$ be the initial solution and define $z(x, t^{0,-}) = z_0(x)$;
- For $n = 0, 1, \ldots, m_h$, the solution at t^{n+1} is given by the following subproblem: find the map $z(x,t)\colon [t^n, t^{n+1}] \to V_h$ such that there holds

$$\Big(z_t, v\Big)_{I_h} = \mathcal{H}(t; z, v) + \Big(f, v\Big)_{I_h}, \quad \forall\, v \in V_h, \tag{4.6a}$$

for any $t \in (t^n, t^{n+1}]$, with the initial solution

$$z(x, t^{n,+}) = z(x, t^{n,-}) + g^n(x). \tag{4.6b}$$

Here $z(x, t^{n,\pm})$ are the two limits from different time directions, as usual.

In (4.6a), the bilinear form $\mathcal{H}(t; \cdot, \cdot)$ and the source term f are the same as that in the original DG method. (4.6b) is called the jump condition, and $g^n(x) \in V_h$ is the jump function. Similar as Proposition 2.1, the solution of subproblem (4.6) is continuously differentiable for any $t \in [t^n, t^{n+1}]$. The solution at t^{n+1} is denoted by $z(x, t^{n+1,-})$.

- The solution at the final time T is defined as $z(x,T) = z(x, t^{m_h+1,-})$.

In this paper, we demand that the jump function $g^n(x)$ for $1 \le n \le m_h$ vanishes everywhere except on the troubled location $\mathrm{TL}(n)$. Moreover, we always set $g^0 \equiv 0$ for $n = 0$.

The next lemma gives a sharp boundedness for the UBFs, which is an essential step to derive the optimal error estimate of the DG method (2.3).

LEMMA 4.1. *The solution of the UBFs satisfies the following sharp boundedness*

$$\|z(T)\|^2_{L^2(\mathbb{R})} \le C \left\{ \|z_0\|^2_{L^2(\mathbb{R})} + \int_0^T \|f(t)\|^2_{L^2(\mathbb{R})}\, \mathrm{d}t + \sum_{1 \le n \le m_h} \|g^n\|^2_{L^2(\mathrm{TE}(n))} \right\}, \tag{4.7}$$

where $C > 0$ is a constant independent of m_h and h.

To prove this lemma, we would like to set up the subsequent three propositions. In this process, we need to fully utilize the geometric structure of the subdivision and the special configuration of the jump functions.

PROPOSITION 4.2. *For $n = 0, 1, \ldots, m_h$, there holds*

$$\|z(t^{n+1,-})\|^2_{L^2(D)} \le e^{C(t^{n+1}-t^n)} \Big(\|z(t^{n,+})\|^2_{L^2(D)} + \int_{t^n}^{t^{n+1}} \|f(t)\|^2_{L^2(D)}\, \mathrm{d}t \Big), \tag{4.8}$$

where $C > 0$ is a constant independent of n, m_h and h, and D is either $\mathbb{R}$ or $\mathrm{TH}(n+1)$.

Proof. Take $D = \mathrm{TH}(n+1)$ as an example to show how to get this proposition, since the proof for $D = \mathbb{R}$ is similar. To this end, we choose in (4.6a) the test function

$$v = z(x,t) \cdot \mathbf{1}_{\mathrm{TH}(n+1)} \in V_h, \quad t \in (t^n, t^{n+1}],$$

where $\mathbf{1}_{\mathrm{TH}(n+1)}$ is the characteristic function of $\mathrm{TH}(n+1)$. This manipulation is reasonable for the mesh-dependent subdivision discussed in the previous subsection, which yields

$$\frac{1}{2}\frac{\mathrm{d}}{\mathrm{d}t}\|z(t)\|^2_{L^2(\mathrm{TH}(n+1))} = \mathcal{H}(t;z,v) + \Big(f, v\Big)_{I_h}, \quad t \in (t^n, t^{n+1}]. \tag{4.9}$$

The boundedness to $\mathcal{H}(t;z,v)$ can be given in the same form as usual; however, the analysis process will be affected by the trajectory's sign to some extent. Below we would like to only present the proof for the case that degenerate points move rightward; see the first two pictures of Figure 3. Letting $j_\star^{n+1}$ be the number of the troubled element $\mathrm{TE}(n+1)$, an integration by parts yields

$$\mathcal{H}(t;z,v) = -\frac{1}{2}\int_{\mathrm{TH}(n+1)} \beta_x z^2 \,\mathrm{d}x - \frac{1}{2}\sum_{j\geq j_\star^{n+1}} \Big|\beta_{j+\frac{1}{2}}\Big| [\![z]\!]^2_{j+\frac{1}{2}} + \Big(\widehat{\beta(t)} z z^+\Big)_{j_\star^{n+1}-\frac{1}{2}}.$$

The first term is bounded by $C\|z\|^2_{L^2(\mathrm{TH}(n+1))}$ and the second term is non-positive. The last term reflects the contribution of the essential subregion, which ensures $\beta_{j_\star^{n+1}-\frac{1}{2}}(t) \leq 0$ due to property (P1). Since the purely upwind flux is used, we have

$$\Big(\widehat{\beta(t)} z z^+\Big)_{j_\star^{n+1}-\frac{1}{2}} = \Big(\beta(t)(z^+)^2\Big)_{j_\star^{n+1}-\frac{1}{2}} \leq 0.$$

Further, an application of Cauchy–Schwarz inequality and Young inequality yields

$$\Big(f, v\Big)_{I_h} = \int_{\mathrm{TH}(n+1)} f z \,\mathrm{d}x \leq \|f\|^2_{L^2(\mathrm{TH}(n+1))} + C\|z\|^2_{L^2(\mathrm{TH}(n+1))}.$$

Substituting the above conclusions into (4.9), we can obtain (4.8) by an application of the Gronwall inequality stated in Lemma 3.1. ∎

Proposition 4.3. *There exists a constant $C > 0$ independent of ε, m_h and h, such that*

$$\|z(T)\|^2_{L^2(\mathbb{R})} \leq e^{CT}\left\{\|z_0\|^2_{L^2(\mathbb{R})} + \int_0^T \|f(t)\|^2_{L^2(\mathbb{R})}\,\mathrm{d}t + \sum_{1\leq n\leq m_h} \mathcal{Y}^n\right\}, \tag{4.10}$$

where ε is an arbitrary positive constant, and

$$\mathcal{Y}^n = \varepsilon\|z(t^{n,-})\|^2_{L^2(\mathrm{TE}(n))} + (1+\varepsilon^{-1})\|g^n\|^2_{L^2(\mathrm{TE}(n))}. \tag{4.11}$$

Proof. The proof of this proposition begins with Proposition 4.2 with $D = \mathbb{R}$. Below we just need to make a careful treatment for the jump condition (4.6b).

Owing to the special configuration of g^n, it is easy to see the following conclusions. For any $n = 1, 2, \ldots, m_h$ and $I_j = \mathrm{TE}(n)$ there holds

$$\|z(t^{n,+})\|^2_{L^2(I_j)} - \|z(t^{n,-})\|^2_{L^2(I_j)} \leq \varepsilon\|z(t^{n,-})\|^2_{L^2(I_j)} + (1+\varepsilon^{-1})\|g^n\|^2_{L^2(I_j)}, \tag{4.12a}$$

and otherwise,

$$\|z(t^{n,+})\|^2_{L^2(I_j)} - \|z(t^{n,-})\|^2_{L^2(I_j)} = 0. \tag{4.12b}$$

In (4.12a) we have used the inequality $(a+b)^2 - a^2 \leq \varepsilon a^2 + (1+\varepsilon^{-1})b^2$ for any a and b, which is implied by Young inequality. Summing up (4.12) over all $j \in \mathbb{Z}$ yields

$$\|z(t^{n,+})\|^2_{L^2(\mathbb{R})} \leq \|z(t^{n,-})\|^2_{L^2(\mathbb{R})} + \mathcal{Y}^n, \quad n \geq 0, \tag{4.13}$$

where we have additionally defined $\mathcal{Y}^0 = 0$ on the basis of (4.11). Substituting this inequality into (4.8) with $D = \mathbb{R}$, we can get for any $0 \le n \le m_h$,

$$\|z(t^{n+1,-})\|^2_{L^2(\mathbb{R})} \le e^{C(t^{n+1}-t^n)}\Big(\|z(t^{n,-})\|^2_{L^2(\mathbb{R})} + \int_{t^n}^{t^{n+1}} \|f(t)\|^2_{L^2(\mathbb{R})}\,\mathrm{d}t + \mathcal{Y}^n\Big).$$

Applying Lemma 3.2 with $\gamma = 1$ and using the initial condition of the UBFs, we complete the proof of Proposition 4.3. ∎

Since the purely upwind numerical flux is applied, the UBFs also form a closed system on the essential subregion. As a conclusion, we are able to set up the following nice result to sharply control the only unknown data in (4.10), namely

$$\sum_{1\le n\le m_h} \|z(t^{n,-})\|^2_{L^2(\mathrm{TE}(n))}.$$

This summation term, referred to as the accumulation of troubled information, can be sharply controlled by the following proposition.

PROPOSITION 4.4. *There exists a constant $C > 0$ independent of m_h and h, such that*

$$\sum_{1\le n\le m_h} \|z(t^{n,-})\|^2_{L^2(\mathrm{TE}(n))} \le e^{CT}\left\{\|z_0\|^2_{L^2(\mathbb{R})} + \int_0^T \|f(t)\|^2_{L^2(\mathbb{R})}\,\mathrm{d}t\right\}. \tag{4.14}$$

Proof. Similarly, the proof of this proposition starts from Proposition 4.2 with $D = \mathrm{TH}(n+1)$, and we need to make a more careful treatment for the jump condition (4.6b).

Let $n \ge 1$. Since $\mathrm{TH}(n+1) \times \{t^n\}$ does not contain any troubled location, there is not any jump and hence we have

$$\|z(t^{n,-})\|_{L^2(\mathrm{TH}(n+1))} = \|z(t^{n,+})\|_{L^2(\mathrm{TH}(n+1))}.$$

With the help of the geometric structure relationship (4.5), one can easily see that

$$\begin{aligned}\|z(t^{n,-})\|^2_{L^2(\mathrm{TH}(n))} &= \|z(t^{n,-})\|^2_{L^2(\mathrm{TH}(n+1))} + \|z(t^{n,-})\|^2_{L^2(\mathrm{TE}(n))}\\ &= \|z(t^{n,+})\|^2_{L^2(\mathrm{TH}(n+1))} + \|z(t^{n,-})\|^2_{L^2(\mathrm{TE}(n))}.\end{aligned} \tag{4.15}$$

Add $e^{C(t^{n+1}-t^n)}\|z(t^{n,-})\|^2_{L^2(\mathrm{TE}(n))}$ on both sides of (4.8) with $D = \mathrm{TH}(n+1)$, and respectively use $e^{C(t^{n+1}-t^n)} \ge 1$ and (4.15) on the left and right sides of the obtained inequality. This implies that

$$\begin{aligned}&\|z(t^{n+1,-})\|^2_{L^2(\mathrm{TH}(n+1))} + \|z(t^{n,-})\|^2_{L^2(\mathrm{TE}(n))}\\ &\qquad\le e^{C(t^{n+1}-t^n)}\Big(\|z(t^{n,-})\|^2_{L^2(\mathrm{TH}(n))} + \int_{t^n}^{t^{n+1}} \|f(t)\|^2_{L^2(\mathrm{TH}(n+1))}\,\mathrm{d}t\Big),\end{aligned} \tag{4.16}$$

holds for $n = 1, \ldots, m_h$.

Recalling the supplementary notations $\mathrm{TH}(0) = \mathrm{TH}(1)$ and $\mathrm{TE}(0) = \emptyset$, as mentioned after (4.5), it follows from the inequality (4.8) with $D = \mathrm{TH}(n+1)$ and $n = 0$ that (4.16) also holds true for $n = 0$. Here we have used the fact that

$$\|z(t^{0,+})\|_{L^2(\mathrm{TH}(1))} = \|z(t^{0,-})\|_{L^2(\mathrm{TH}(0))} = \|z_0\|_{L^2(\mathrm{TH}(0))}, \tag{4.17}$$

due to the initial condition of the UBFs.

Using Lemma 3.2 with $\gamma = 1$ for (4.16), which holds for $n = 0, 1, \ldots, m_h$, we arrive at

$$\|z(t^{m_h+1,-})\|^2_{L^2(\mathrm{TH}(m_h+1))} + \sum_{1\le n\le m_h} \|z(t^{n,-})\|^2_{L^2(\mathrm{TE}(n))} \\ \le e^{CT}\Big(\|z_0\|^2_{L^2(\mathrm{TH}(0))} + \sum_{0\le n\le m_h} \int_{t^n}^{t^{n+1}} \|f(t)\|^2_{L^2(\mathrm{TH}(n+1))}\,\mathrm{d}t\Big),$$

where (4.17) is also used. This completes the proof of Proposition 4.4 by dropping the first term on the left hand side and enlarging the integration domain on the right hand side. ∎

Now we can prove Lemma 4.1 by collecting Proposition 4.3 with $\varepsilon = 1$ and Proposition 4.4. The case with a small ε will be used for multiple trajectories; see (5.3) in Section 5 below.

REMARK 4.1. *If all $g^n \equiv 0$, the UBFs reduce to the original DG method (2.3), and Lemma 4.1 implies the standard stability result.*

REMARK 4.2. *It is worth stressing the importance of the essential subregion and the relevant concepts. Without the help of them, we might merely adopt the traditional technique (triangle inequality and Young inequality) to derive a rough estimate*

$$\|z(t^{n,+})\|^2_{L^2(\mathbb{R})} \le (\|z(t^{n,-})\|_{L^2(\mathbb{R})} + \|g^n\|_{L^2(\mathbb{R})})^2 \le (1+\epsilon)\|z(t^{n,-})\|^2_{L^2(\mathbb{R})} + (1+\epsilon^{-1})\|g^n\|^2_{L^2(\mathbb{R})},$$

where $\epsilon \le 1$ is an arbitrary positive constant. Substituting this inequality into (4.8) with $D = \mathbb{R}$ and applying Lemma 3.2 with $\gamma = 1+\epsilon$, we can obtain

$$\|z(T)\|^2_{L^2(\mathbb{R})} \le (1+\epsilon)^{m_h+1} e^{CT}\left[\|z_0\|^2_{L^2(\mathbb{R})} + \int_0^T \|f(t)\|^2_{L^2(\mathbb{R})}\,\mathrm{d}t + \frac{1}{\epsilon}\sum_{1\le n\le m_h} \|g^n\|^2_{L^2(\mathbb{R})}\right], \tag{4.18}$$

where $C > 0$ is a constant independent of h, m_h and ϵ. Since $\epsilon = 1/m_h$ is the optimal parameter to control $(1+\epsilon)^{m_h}$ and minimize $(1+\epsilon)^{m_h}/\epsilon$, the obtained boundedness result in this way involves an unsatisfactory amplification factor $m_h = \mathcal{O}(h^{-1})$ in the last term, which is different from the sharp boundedness of UBFs in Lemma 4.1.

4.3. Optimal error estimate. In this subsection, we propose the explicit definition of the time-dependent projection and complete the proof of Theorem 2.1 under Assumption (B).

4.3.1. The time-dependent projection. After we have determined the subdivision as in Subsection 4.1, we would like to define the time-dependent projection operator $\mathbb{Q}(t)$ based on two types of GR projections and the distribution of location signs.

DEFINITION 4.2. *Let $w(x)$ be a given smooth function on $\mathbb{R}$. For any parameter $t \in [0, T]$, the projection $\mathbb{Q}(t)w(x) \in V_h$ is defined element by element, namely*

$$\mathbb{Q}(t)w(x)\Big|_{I_j} = \begin{cases} \mathbb{G}_{j,+}w(x) \\ \mathbb{G}_{j,-}w(x) \end{cases} \quad \text{if the location sign of } I_j(t) \text{ is } \begin{matrix} \text{positive;} \\ \text{negative.} \end{matrix}$$

At each troubled moment t^n, the projection $\mathbb{Q}(t^n)w(x)$ is double valued for $n = 1, 2, \ldots, m_h$, which should be understood as two limits from different time directions and denoted by $\mathbb{Q}(t^{n,\pm})w(x)$.

Let $\mathbb{Q}^\perp(t)w = w - \mathbb{Q}(t)w$ be the projection error, which are allowed to have two different limits at each troubled moment. Two approximation properties are given below.

PROPOSITION 4.5. *For $t \in [0, T]$, there holds*

$$\|\mathbb{Q}^\perp(t)w\|_{L^2(I_j)} + \|\mathbb{Q}^\perp(t)w\|_{L^2(\partial I_j)} \le Ch^{k+1}\|w\|_{H^{k+1}(I_j)}, \tag{4.19}$$

where the bounding constant $C > 0$ is independent of j, t, h and w.

Proof. It is nothing but the approximation property (3.4) of GR projections. ∎

PROPOSITION 4.6. *For $t \in [0,T]$, the DG discretization operator satisfies*

$$\left|\mathcal{H}(t;\mathbb{Q}^{\perp}(t)w,v)\right| \le Ch^{k+1}\|w\|_{H^{k+1}(\mathbb{R})}\|v\|_{L^2(\mathbb{R})}, \quad \forall\, v \in V_h, \tag{4.20}$$

where the bounding constant $C>0$ is independent of t, h and w.

Proof. Similar proposition has been discussed in many literatures, for example, [17], so we only present the proof sketch here. Due to the definition of GR projections, it is easy to see

$$\mathcal{H}(t;\mathbb{Q}^{\perp}(t)w,v) = \Big([\beta(t)-\bar{\beta}(t)]\mathbb{Q}^{\perp}(t)w, v_x\Big)_{I_h} + \Big\langle \widehat{\beta(t)\mathbb{Q}^{\perp}(t)w}, [\![v]\!]\Big\rangle_{\Gamma_h},$$

where $\bar{\beta}(t)$ is the piecewise constant approximation function of $\beta(t)$ such that $|\beta(t)-\bar{\beta}(t)| \le Ch$ holds everywhere. Each term is bounded by the right hand side of (4.20), if we use Proposition 4.5, the inverse inequality (3.5) and the following two facts. One is the exact collocation at those element endpoints far away the transition subregion and the other is $\beta = O(h)$ at those nearby the transition subregion. ∎

REMARK 4.3. *Note that the above two propositions always hold true, no matter how we define the location signs nearby the transition subregion.*

It is easy to see that the jump of projection error at troubled location satisfy

$$\|\mathbb{Q}^{\perp}(t^{n,+})w - \mathbb{Q}^{\perp}(t^{n,-})w\|_{L^2(\mathrm{TE}(n))} \le Ch^{k+1}\|w\|_{H^{k+1}(\mathrm{TE}(n))}, \quad 1 \le n \le m_h, \tag{4.21}$$

due to the triangle inequality and Proposition 4.5. We remark that the order in this inequality cannot be improved in general.

4.3.2. Final proof. Now we have prepared all the materials to carry out the optimal error estimate. Along the standard analysis line of finite element methods, we would like to introduce the error decomposition

$$\mathcal{E}(t) = u(t) - U(t) = \underbrace{[u(t) - \mathbb{Q}(t)U(t)]}_{\xi(t)\in V_h} - \underbrace{[U(t) - \mathbb{Q}(t)U(t)]}_{\eta(t)\triangleq\mathbb{Q}^{\perp}(t)U(t)}, \tag{4.22}$$

which has essential differences despite of its similar form. As mentioned in Subsection 2.2, we know that $U(t), u(t)$ and hence $\mathcal{E}(t)$ are continuous with respect to time. However, Definition 4.2 shows that $\mathbb{Q}(t)U(t)$ and hence $\eta(t)$ are discontinuous at troubled moments. Together with (4.22) and the continuity of $\mathcal{E}(t)$, we know that $\xi(t)$ is also discontinuous at troubled moments.

It follows from the approximation property in Proposition 4.5 that

$$\|\eta(t)\|_{L^2(\mathbb{R})} \le Ch^{k+1}, \quad t \in [0,T], \tag{4.23}$$

which does not cause any difficulty in obtaining the optimal error estimate. We remark that $\eta(t)$ is understood as two limits from different directions at troubled moments.

Due to the triangle inequality and (4.23), we only need to pay attention to obtaining the optimal estimate of $\|\xi(T)\|_{L^2(\mathbb{R})}$. Since the original DG method (2.3) is consistent, the error decomposition (4.22) leads to the following error equations with respect to $\xi(t)$:

- At $t^0 = 0$, the initial solution $\xi(t^0) = \xi(t^{0,-})$ is well defined;
- Let $0 \le n \le m_h$. In each time interval $t \in (t^n, t^{n+1}]$, there holds for any $v \in V_h$ that

$$\Big(\xi_t(t), v\Big)_{I_h} = \mathcal{H}(t;\xi(t),v) + \Big(\mathcal{Z}(t), v\Big)_{I_h}, \tag{4.24a}$$

  where $\mathcal{Z}(t) \in V_h$ is uniquely determined by $(\mathcal{Z}(t),v)_{I_h} = (\eta_t(t),v)_{I_h} - \mathcal{H}(t;\eta(t),v)$ for any $v \in V_h$.

- Let $1 \le n \le m_h$. At each troubled moment $t = t^n$, there holds the jump condition

$$\xi(t^{n,+}) - \xi(t^{n,-}) = \eta(t^{n,+}) - \eta(t^{n,-}) \equiv \mathcal{G}^n, \tag{4.24b}$$

due to the fact that $e(t^{n,+}) = e(t^{n,-})$. Regarding the setting of the initial solution, (4.24b) can be extended to $n = 0$ with a supplementary notation $\mathcal{G}^n = 0$.

Clearly, these error equations have the same form as the UBFs, proposed in Subsection 4.2. Hence, we are able to use the sharp boundedness as stated in Lemma 4.1 to get

$$\|\xi(T)\|^2_{L^2(\mathbb{R})} \le C \left\{ \|\xi(0)\|^2_{L^2(\mathbb{R})} + \int_0^T \|\mathcal{Z}(t)\|^2_{L^2(\mathbb{R})}\,\mathrm{d}t + \sum_{1\le n\le m_h} \|\mathcal{G}^n\|^2_{L^2(\mathrm{TE}(n))} \right\}. \tag{4.25}$$

The three terms inside the brace can be estimated as follows.

It follows from Proposition 4.5 and the assumption on the initial solution (2.6) that

$$\|\xi(0)\|_{L^2(\mathbb{R})} \le \|u_0 - U_0\|_{L^2(\mathbb{R})} + \|\mathbb{Q}(0)U_0 - U_0\|_{L^2(\mathbb{R})} \le Ch^{k+1}, \tag{4.26}$$

where the triangle inequality is used. On each small time interval separated by troubled moments, it is easy to verify that

$$\eta_t(t) = \mathbb{Q}^{\perp}(t)U_t(t),$$

since the detailed type of GR projections on each element remains unchanged in time. Hence we can use Propositions 4.5 and 4.6 to get

$$\|\mathcal{Z}(t)\|_{L^2(\mathbb{R})} \le Ch^{k+1}\Big(\|U_t(t)\|_{H^{k+1}(\mathbb{R})} + \|U(t)\|_{H^{k+1}(\mathbb{R})}\Big) \le Ch^{k+1} \tag{4.27}$$

on every time interval, which gives the estimate to the second term inside the brace of (4.25). In order to derive the optimal estimate to the last term in (4.25), the accumulation of the jumps of projection errors, we need the following result for the exact solution.

LEMMA 4.2. *Assume that (2.7) and (2.8) hold true, then the exact solution of the model problem (2.1) satisfies*

$$\sum_{1\le n\le m_h} \|U(t^n)\|^2_{H^{k+1}(\mathrm{TE}(n))} \le C,$$

where the bounding constant $C > 0$ is independent of m_h, h, U and f.

Proof. By an analogous and simpler argument as that in the proof of Proposition 4.4, we can use the induction procedure by taking the spatial derivative, up to $(k+1)$th order, of the hyperbolic equation and the initial condition in (2.1). Finally, we get

$$\sum_{1\le n\le m_h} \|U(t^n)\|^2_{H^{k+1}(\mathrm{TE}(n))} \le C \left\{ \|U_0\|^2_{H^{k+1}(\mathrm{TH}(0))} + \sum_{0\le n\le m_h} \int_{t^n}^{t^{n+1}} \|f(t)\|^2_{H^{k+1}(\mathrm{TH}(n+1))}\,\mathrm{d}t \right\},$$

where the properties of the essential subregion still play an important role. This finishes the proof of Lemma 4.2 by noticing (2.7) and (2.8). ∎

By (4.21), (4.24b) and Lemma 4.2, we have

$$\sum_{1\le n\le m_h} \|\mathcal{G}^n\|^2_{L^2(\mathrm{TE}(n))} \le Ch^{2k+2} \sum_{1\le n\le m_h} \|U(t^n)\|^2_{H^{k+1}(\mathrm{TE}(n))} \le Ch^{2k+2}. \tag{4.28}$$

Substituting (4.26)–(4.28) into (4.25), we have the expected conclusion $\|\xi(T)\|_{L^2(\mathbb{R})} \le Ch^{k+1}$, which, together with (4.23), gives the optimal error estimate. Now we have completed the proof of Theorem 2.1 for the case with a single trajectory.

REMARK 4.4. *For the case that degenerate points form a vertical trajectory, the above analysis framework still works since the troubled moments and the troubled locations are empty.*

5. Proof of Theorem 2.1 for multiple trajectories. In this section we extend our analysis framework to multiple trajectories. The new difficulty we have to face is that the adjacent distances could have different sizes on a time interval.

Due to Assumption (A2), we know that, for any $h > 0$, there always exist a finite number of time intervals such that every adjacent distance $d_i(t)$ has the clear state of either large (if $d_i(t) \geq 3h$ there) or small (if $d_i(t) \leq 3h$ there). Motivated by the discussions at the end of Subsection 2.3, we can further simplify Assumption (A2) on each time interval as follows.

- All trajectories in (2.10) are continuously differentiable and strictly monotone, and they do not intersect with each other except at the initial time or the final time;
- Each adjacent distance has one clear state of either large or small;
- The flow speed changes the sign when passing through each trajectory.

Similar to the assumption for the case of a single trajectory, we also remove here the trivial case that the trajectory is a vertical line.

REMARK 5.1. *The length of the above involved time interval may depend on the mesh size, due to the definition of the states of adjacent distances. This phenomenon is entirely different to that for a single trajectory.*

Roughly speaking, the optimal error estimate for multiple trajectories can be obtained along the same line as that for a single trajectory. However, in this process we have to address two new issues. One is the proper definition of the location sign, in which the combination techniques for adjacent subregions are updated. The other is how to prove the sharp boundedness of the UBFs, which involve jump functions on multiple groups of troubled locations.

5.1. Definition of the location sign. In this subsection, we would like to update some concepts and techniques, to deal with the hybrid of various states of adjacent distances on each time interval. They are explicitly illustrated in the following three subsections.

5.1.1. The case that all adjacent distances are small. This case needs only to be considered when the trajectories intersect at an endpoint of the time interval, as h goes to zero. To well describe our strategy in this case, we would like to promote some notations from one trajectory to multiple ones.

- Denote by $\Omega_\star$ the generalized transition subregion, which is expanded and connected by the transition subregions of all trajectories.
- Beside $\Omega_\star$, the left and right subregions are still denoted by $\Omega_{\rm L}$ and $\Omega_{\rm R}$. Their subregion signs are easily defined as the sign of the flow speed there.

Due to Definition 4.1, we only need to properly define the subregion sign of $\Omega_\star$. Basically, the strategy proposed in this paper is to ignore the existence of some trajectories and pick up a single trajectory or nothing there. The detailed treatments depend on the parity of the trajectories' number.

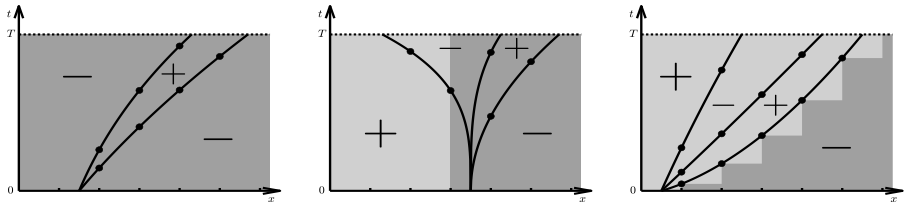

FIG. 4. *All adjacent distances are small. The extended subregions are marked by light and dark shadow. Left: even trajectories; Middle: odd trajectories without the same moving directions; Right: odd trajectories with the same moving direction.*

It is easy to handle the case that the number of trajectories is even. Due to the alternative distribution of the flow direction, the subregions $\Omega_{\rm L}$ and $\Omega_{\rm R}$ have the same subregion sign. In this

case, our strategy is to ignore all trajectories and define the subregion sign of $\Omega_\star$ by this sign; see the left picture of Figure 4.

REMARK 5.2. *The excluded case that the flow speed has the same sign on both sides of a trajectory can be understood as two totally overlapping trajectories.*

For the case of odd number of trajectories, the subregions $\Omega_{\rm L}$ and $\Omega_{\rm R}$ have the opposite subregion signs. In this case, our strategy is to pick out one special trajectory and ignore the existence of the others. For this purpose, we need to carry out the following operations:

1. Arbitrarily select a trajectory and find its transition subregion, denoted by $\Omega_\star^{\rm pick}$.
2. For the left and right subregions, respectively denoted by $\Omega_{\rm L}^{\rm pick}$ and $\Omega_{\rm R}^{\rm pick}$, we ignore the existence of the other trajectories and forcefully define their subregion signs by those of $\Omega_{\rm L}$ and $\Omega_{\rm R}$, respectively.
3. Along the same process as for a single trajectory, we determine the subdivision of the computational domain and properly define the subregion sign of $\Omega_\star^{\rm pick}$. The obtained essential subregion is denoted by $\Omega_{\star\star}^{\rm pick}$.
4. If the other trajectories that have been ignored simultaneously lie inside or outside of $\Omega_{\star\star}^{\rm pick}$, then the selected trajectory is the correct one to accomplish our purpose. This judgment criteria implies that the candidate choices must be taken from two trajectories nearby the boundary of the generalized transition region $\Omega_\star$.

A typical example is plotted in the right picture of Figure 4, where the total number of troubled moments achieves $\mathcal{O}(h^{-1})$, as stated in Proposition 4.1 for a single trajectory.

Below we give a comment on the special case that the number of trajectories is odd and the moving directions are different; see the middle picture of Figure 4. Since the moving distance of each trajectory is $\mathcal{O}(h)$, the total number of troubled moments is $\mathcal{O}(1)$. Hence, the optimal error estimate for this case does not encounter any difficulties. In order to focus on our attention to address the main difficulties, we would like to provide a simple treatment as follows. Because there exists a vertical line located at an element endpoint and intersected with $\Omega_\star$, the theoretical analysis for this case can be carried out along the the same line as that for a vertical trajectory of degenerate points. That is, our strategy now is to replace all trajectories by the aforementioned vertical line, and define the subregion signs for the left and right zones by those of $\Omega_{\rm L}$ and $\Omega_{\rm R}$, respectively.

5.1.2. The case that all adjacent distances are large. Now we turn to the other extreme case that all adjacent distances are large. In this case, the strategy is the same as that for one single trajectory. In more detail, we derive the subdivision and a group of troubled locations for each trajectory, as we have done in Subsection 4.1. Since all adjacent distances are large, the staircase-shape boundaries of the essential subregions do not intersect with each other, and they divide the computation stripe (the Cartesian product of $\mathbb{R}$ and the considered time interval) into mesh-dependent zones with alternating positive and negative subregion signs.

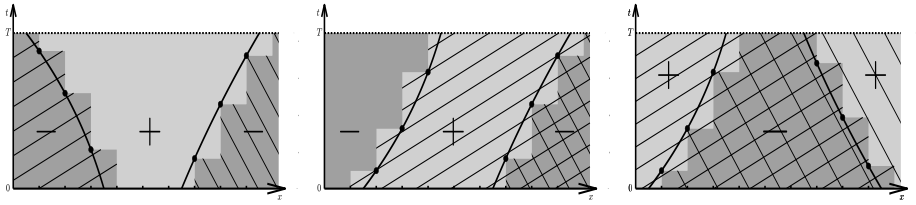

FIG. 5. *All adjacent distances are large. Three extended subregions are marked by light and dark shadow, and two essential subregions are marked by slash and backslash lines.*

Typical examples for this case are plotted in Figure 5, where, from left to right, the essential subregion for any two trajectories have three states: separation, inclusion, and intersection (not inclusive).

5.1.3. The case that adjacent distances have mixed states. Finally we consider the general case that different states arise at the same time. Roughly speaking, the treatment for this case is the integrated application of the above two strategies.

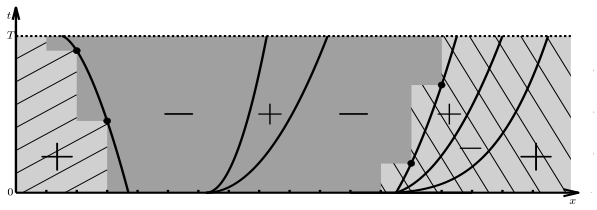

FIG. 6. *The adjacent distances have different states. Six trajectories (solid lines) are divided into three groups. Three extended subregions are marked by light and dark shadow, and two essential subregions are marked by slash and backslash lines.*

This process is split into three steps. First, we divide the trajectories from left to right into several groups by the following rules. If the adjacent distance is small, then both trajectories related to this distance are in the same group; otherwise, let the right trajectory form a new group. In other words, the distance between different groups of trajectories is large. See Figure 6 as an example.

Then, we select a single trajectory or nothing from every group of trajectories. If there are multiple trajectories in the same group, we just need to locally execute the similar operations as we have done for the extreme case that all adjacent distances are small. Keep in mind that the sign of the flow speed might be locally modified by the newly-defined subregion signs. Finally, we derive the subdivision and troubled locations for each selected trajectory, as that in the extreme case that all adjacent distances are large.

5.2. A sharp boundedness of the UBFs. On any considered time interval, we can similarly define the UBFs by introducing the jump functions on all groups of troubled locations. For the convenience of statement, we denote the time interval by $[0, T]$, and thus the UBFs has the same representations as that in Subsection 4.2.

Actually, the sharp boundedness of the UBFs is stated as the same as that in Lemma 4.1, where the accumulation of troubled information is enlarged to multiple trajectories. The proofs are analogous to those in Subsection 4.2, and the main modification comes from how to prove the boundedness about the accumulation of troubled information along all trajectories, as an extension of Proposition 4.4.

To show the updated technique for achieving the above aim, we would like in what follows to take Figure 5 as an example, which has two trajectories with a large adjacent distance. Each trajectory yields a series of concepts as mentioned previously, for example, the troubled moments and locations, the subdivision, and the essential subregion. For simplicity of statement, the trajectory under consideration is named as the master trajectory and the other trajectory is referred to as the slave one. For the ease of reading, we add a tilde to those notations regarding the slave trajectory.

Let $\{t^n : 1 \le n \le m_h\}$ and $\tilde{S} = \{t^{\tilde{n}} : 1 \le \tilde{n} \le \tilde{m}_h\}$ be the troubled moments for the master and the slave trajectories, respectively. All moments belong to $(0, T)$ and are arranged in ascending order in each set. We remark that the above notations can be similarly extended to $n = 0, m_h + 1$ and $\tilde{n} = 0, \tilde{m}_h + 1$.

Denoting $\tilde{S}_n = \{t^{\tilde{n}} \in \tilde{S} : t^n \le t^{\tilde{n}} < t^{n+1}\}$, we can update the result of Proposition 4.2 to

$$\|z(t^{n+1,-})\|^2_{L^2(\mathrm{TH}(n+1))} \le e^{C(t^{n+1}-t^n)}\Big(\|z(t^{n,+})\|^2_{L^2(\mathrm{TH}(n+1))} + \cdots + \sum_{t^{\tilde{n}} \in \tilde{S}_n \setminus \{t^n\}} \widetilde{\mathcal{Y}}^{\tilde{n}}\Big), \tag{5.1}$$

where $0 \le n \le m_h$ and the skipped part is the same as before. Here $\widetilde{\mathcal{Y}}^{\tilde{n}}$ is defined similarly as that in Proposition 4.3 with the integration domain being $\widetilde{\mathrm{TE}}(\tilde{n})$.

For the case that the essential subregions are separated, $\widetilde{\mathrm{TE}}(\tilde{n}) = \emptyset$ and so inequality (5.1) holds obviously. For the other cases, we can get (5.1) along the same line as that of Proposition 4.2. As the main modification in this process, those jump functions at troubled moments lying in $S_n \backslash \{t^n\}$ can be similarly controlled as in that of Proposition 4.3. Remark that this operation will also be used in the next step to get (5.2), if $t^n \in \tilde{S}_n$.

In (5.1), the integration domain for the two norms on both sides remains unchanged. Along the same line as that of Proposition 4.4, we can use the geometric structure relationship (4.5) of the master trajectory and get a similar result

$$\sum_{1\le n\le m_h} \|z(t^{n,-})\|^2_{L^2(\mathrm{TE}(n))} \le e^{CT}\left\{\varepsilon \sum_{1\le \tilde{n}\le \widetilde{m}_h} \|z(t^{\tilde{n},-})\|^2_{L^2(\widetilde{\mathrm{TE}}(\tilde{n}))} + \mathcal{R}_1 + \mathcal{R}_2\right\}, \tag{5.2}$$

where $\mathcal{R}_1 = (1+\varepsilon^{-1}) \sum_{1\le \tilde{n}\le \widetilde{m}_h} \|g^{\tilde{n}}\|^2_{L^2(\widetilde{\mathrm{TE}}(\tilde{n}))}$ and

$$\mathcal{R}_2 = \|z_0\|^2_{L^2(\mathrm{TH}(0))} + \sum_{0\le n\le m_h} \int_{t^n}^{t^{n+1}} \|f(t)\|^2_{L^2(\mathrm{TH}(n+1))}\,\mathrm{d}t$$

can be further bounded by enlarging the integration domain to $\mathbb{R}$. Recall that the total number of all considered trajectories is $s_\star$, and, in Figure 5, it is equal to 2. Collecting this kind of results for all trajectories, and letting ε be a small enough constant independent of h such as

$$e^{CT}\varepsilon(s_\star - 1) \le \frac{1}{2}, \tag{5.3}$$

we can get the sharp boundedness for all troubled information of the numerical solution.

6. Numerical experiments. In this section we present some numerical experiments to verify the optimal convergence order. Two examples are considered below.

EXAMPLE 6.1. *Let $\beta(x,t) = (x - \sin \pi t)/(x^2+1)$. There is a single trajectory of degenerate points $x_\star(t) = \sin \pi t$, which changes the moving direction at $t = 0.5$.*

EXAMPLE 6.2. *Let $\beta(x,t) = (x-\sin \pi t)(x-t^3)/(x^4+1)$. There are two intersecting trajectories of degenerate points $\ell_1(t) = \sin \pi t$ and $\ell_2(t) = t^3$.*

In all experiments, the exact solution is defined as

$$U(x,t) = \begin{cases} [\sin(\pi(x-t))]^9, & \text{if } x - t \in [-2,2], \\ 0, & \text{otherwise,} \end{cases} \tag{6.1}$$

determining the initial solution and the source term. Take the final time $T = 1$ and set the computational region to be $[-10,10]$. Let $k = 0,1,2,3$, and adopt the four-stage-and-fourth-order Runge–Kutta time-marching [22, Eq. (2.10)], with the time step $\tau = 0.1h_{\min}$ and $h_{\min}$ being the minimum of all element lengths. Both uniform and non-uniform meshes are considered, where the non-uniform mesh is generated by randomly perturbing the uniform mesh nodes by at most 10%. In Tables 1 and 2, we present the errors and convergence orders in L^2 and L^∞ norm for two considered examples, where J is the number of elements. The optimal order in all cases is clearly observed.

7. Conclusion. In this paper, we consider one-dimensional linear hyperbolic equation, and pay attention to the case where the flow speed has different signs and the degenerate points move along space-time curves. A novel analysis framework is proposed to rigorously prove the optimal error estimate of the DG method with the purely upwind numerical flux. The key ingredient of the proof is the mesh-dependent subdivision of the computational domain and the union of bilinear forms with jump conditions on troubled locations, for which a sharp boundedness for the accumulation of jump terms is established. In future work, we will extend our work to DG methods with upwind-biased

TABLE 1
Example 6.1. The L^2-norm error and convergence order.

k	J	uniform mesh				non-uniform mesh			
		L^2-error	order	L^∞-error	order	L^2-error	order	L^∞-error	order
0	2560	8.41E-02		4.16E-02		8.53E-02		4.17E-02	
	5120	4.27E-02	0.98	2.10E-02	0.99	4.33E-02	0.98	2.12E-02	0.97
	10240	2.16E-02	0.99	1.05E-02	0.99	2.18E-02	0.99	1.06E-02	1.00
	20480	1.08E-02	0.99	5.28E-03	1.00	1.10E-02	0.99	5.33E-03	0.99
	40960	5.44E-03	1.00	2.64E-03	1.00	5.51E-03	0.99	2.66E-03	1.00
1	640	1.78E-02		1.44E-02		1.82E-02		1.56E-02	
	1280	4.54E-03	1.97	3.62E-03	2.00	4.75E-03	1.94	4.97E-03	1.65
	2560	1.14E-03	1.99	9.05E-04	2.00	1.18E-03	2.01	1.13E-03	2.14
	5120	2.86E-04	2.00	2.26E-04	2.00	2.95E-04	2.00	2.99E-04	1.91
	10240	7.16E-05	2.00	5.65E-05	2.00	7.37E-05	2.00	7.40E-05	2.01
2	640	7.21E-04		6.11E-04		7.65E-04		8.04E-04	
	1280	8.60E-05	3.07	7.54E-05	3.02	9.33E-05	3.04	1.15E-04	2.80
	2560	1.06E-05	3.01	9.17E-06	3.04	1.15E-05	3.02	1.52E-05	2.93
	5120	1.33E-06	3.00	1.14E-06	3.01	1.41E-06	3.03	1.73E-06	3.13
	10240	1.66E-07	3.00	1.43E-07	3.00	1.78E-07	2.98	2.32E-07	2.89
3	640	2.45E-05		2.68E-05		2.67E-05		3.35E-05	
	1280	1.49E-06	4.04	1.59E-06	4.07	1.67E-06	4.00	2.41E-06	3.79
	2560	8.96E-08	4.06	9.91E-08	4.00	9.87E-08	4.08	1.42E-07	4.09
	5120	5.51E-09	4.02	6.12E-09	4.02	6.17E-09	4.00	1.14E-08	3.64
	10240	3.43E-10	4.01	3.80E-10	4.01	3.85E-10	4.00	6.92E-10	4.04

TABLE 2
Example 6.2. The L^2-norm error and convergence order.

k	J	uniform mesh				non-uniform mesh			
		L^2-error	order	L^∞-error	order	L^2-error	order	L^∞-error	order
0	2560	4.09E-01		2.50E-01		4.11E-01		2.51E-01	
	5120	2.33E-01	0.81	1.45E-01	0.79	2.35E-01	0.81	1.46E-01	0.79
	10240	1.26E-01	0.89	7.83E-02	0.88	1.27E-01	0.89	7.92E-02	0.88
	20480	6.56E-02	0.94	4.08E-02	0.94	6.60E-02	0.94	4.14E-02	0.94
	40960	3.35E-02	0.97	2.09E-02	0.97	3.37E-02	0.97	2.12E-02	0.97
1	640	2.09E-02		1.34E-02		2.15E-02		1.50E-02	
	1280	4.74E-03	2.14	3.58E-03	1.91	4.94E-03	2.12	3.86E-03	1.96
	2560	1.15E-03	2.04	9.04E-04	1.99	1.20E-03	2.04	1.14E-03	1.76
	5120	2.87E-04	2.01	2.26E-04	2.00	2.97E-04	2.02	2.89E-04	1.98
	10240	7.16E-05	2.00	5.65E-05	2.00	7.40E-05	2.00	8.03E-05	1.85
2	640	7.61E-04		5.80E-04		8.52E-04		7.38E-04	
	1280	9.05E-05	3.07	8.27E-05	2.81	1.00E-04	3.09	1.12E-04	2.72
	2560	1.07E-05	3.07	9.17E-06	3.17	1.16E-05	3.11	1.33E-05	3.08
	5120	1.33E-06	3.01	1.14E-06	3.00	1.41E-06	3.04	1.71E-06	2.96
	10240	1.66E-07	3.00	1.43E-07	3.00	1.78E-07	2.99	2.32E-07	2.88
3	640	2.98E-05		2.54E-05		3.31E-05		3.05E-05	
	1280	1.59E-06	4.23	1.52E-06	4.06	1.78E-06	4.22	2.27E-06	3.75
	2560	9.06E-08	4.13	9.67E-08	3.97	1.01E-07	4.14	1.52E-07	3.90
	5120	5.52E-09	4.04	6.07E-09	3.99	6.18E-09	4.03	1.10E-08	3.78
	10240	3.43E-10	4.01	3.84E-10	3.98	3.86E-10	4.00	6.90E-10	4.00

numerical fluxes, and to problems with different boundary conditions and multi-dimensional cases. The extension to the fully discrete methods will also be considered.

REFERENCES

[1] J. Ai, Y. Xu, C.-W. Shu, and Q. Zhang, L^2 *error estimate to smooth solutions of high order Runge-Kutta discontinuous Galerkin method for scalar nonlinear conservation laws with and without sonic points*, SIAM J. Numer. Anal., 60 (2022), pp. 1741–1773.

[2] S. Benzoni-Gavage and D. Serre, *Multidimensional hyperbolic partial differential equations: first-order systems and applications*, Oxford Mathematical Monographs, Oxford University Press, 2007.
[3] D. Bouche, J.-M. Ghidaglia, and F. P. Pascal, *Error estimate for the upwind finite volume method for the nonlinear scalar conservation law*, J. Comput. Appl. Math., 235 (2011), pp. 5394–5410.
[4] ———, *An optimal error estimate for upwind finite volume methods for nonlinear hyperbolic conservation laws*, Appl. Numer. Math., 61 (2011), pp. 1114–1131.
[5] H. Brezis, *Functional Analysis, Sobolev Spaces and Partial Differential Equations*, Springer New York, 2010.
[6] P. Castillo, B. Cockburn, D. Schötzau, and C. Schwab, *Optimal a priori error estimates for the hp-version of the local discontinuous Galerkin method for convection-diffusion problems*, Math. Comp., 71 (2002), pp. 455–478.
[7] P. G. Ciarlet, *The finite element method for elliptic problems*, North-Holland Publishing Co., Amsterdam, New York, Oxford, 1978.
[8] B. Cockburn, *An introduction to the discontinuous Galerkin method for convection-dominated problems*, in Advanced numerical approximation of nonlinear hyperbolic equations, Springer, 1998, pp. 151–268.
[9] ———, *Discontinuous Galerkin methods for convection-dominated problems*, in High-order methods for computational physics, vol. 9 of Lect. Notes Comput. Sci. Eng., Springer, Berlin, 1999, pp. 69–224.
[10] B. Cockburn, S. Hou, and C.-W. Shu, *The Runge-Kutta local projection discontinuous Galerkin finite element method for conservation laws. IV. The multidimensional case*, Math. Comp., 54 (1990), pp. 545–581.
[11] B. Cockburn, S. Y. Lin, and C.-W. Shu, *TVB Runge-Kutta local projection discontinuous Galerkin finite element method for conservation laws. III. One-dimensional systems*, J. Comput. Phys., 84 (1989), pp. 90–113.
[12] B. Cockburn and C.-W. Shu, *TVB Runge-Kutta local projection discontinuous Galerkin finite element method for conservation laws. II. General framework*, Math. Comp., 52 (1989), pp. 411–435.
[13] ———, *The Runge-Kutta local projection P^1-discontinuous-Galerkin finite element method for scalar conservation laws*, RAIRO Modél. Math. Anal. Numér., 25 (1991), pp. 337–361.
[14] ———, *The Runge-Kutta discontinuous Galerkin method for conservation laws. V. Multidimensional systems*, J. Comput. Phys., 141 (1998), pp. 199–224.
[15] S. S. Dragomir, *Some Gronwall type inequalities and applications*, Nova Science Publishers, Inc., Hauppauge, NY, 2003.
[16] P. Lasaint and P. Raviart, *On a finite element method for solving the neutron transport equation*, in Mathematical Aspects of Finite Elements in Partial Differential Equations, Academic Press, 1974, pp. 89–123.
[17] J. Li, D. Zhang, X. Meng, and B. Wu, *Analysis of discontinuous Galerkin methods with upwind-biased fluxes for one dimensional linear hyperbolic equations with degenerate variable coefficients*, J. Sci. Comput., 78 (2019), pp. 1305–1328.
[18] J. Li, D. Zhang, X. Meng, B. Wu, and Q. Zhang, *Discontinuous Galerkin methods for nonlinear scalar conservation laws: generalized local Lax-Friedrichs numerical fluxes*, SIAM J. Numer. Anal., 58 (2020), pp. 1–20.
[19] M. Liu, B. Wu, and X. Meng, *Optimal error estimates of the discontinuous Galerkin method with upwind-biased fluxes for 2D linear variable coefficients hyperbolic equations*, J. Sci. Comput., 83 (2020). Paper No. 9.
[20] X. Meng, C.-W. Shu, and B. Wu, *Optimal error estimates for discontinuous Galerkin methods based on upwind-biased fluxes for linear hyperbolic equations*, Math. Comp., 85 (2016), pp. 1225–1261.
[21] W. H. Reed and T. R. Hill, *Triangular mesh methods for the neutron transport equation*, Los Alamos Scientific Laboratory report LA-UR-73-479, 1973.
[22] C.-W. Shu and S. Osher, *Efficient implementation of essentially nonoscillatory shock-capturing schemes*, J. Comput. Phys., 77 (1988), pp. 439–471.
[23] S. Wollman and E. Ozizmir, *Numerical approximation of the one-dimensional Vlasov-Poisson system with periodic boundary conditions*, SIAM J. Numer. Anal., 33 (1996), pp. 1377–1409.
[24] Y. Xing, X. Zhang, and C.-W. Shu, *Positivity-preserving high order well-balanced discontinuous galerkin methods for the shallow water equations*, Advances in Water Resources, 33 (2010), pp. 1476–1493.
[25] M. Xu, Y. Yuan, W. Cao, and Q. Zou, *Analysis of two any order spectral volume methods for 1-D linear hyperbolic equations with degenerate variable coefficients*, J. Comp. Math., (2023). Online.
[26] Y. Xu, C.-W. Shu, and Q. Zhang, *Stability analysis and error estimate of the explicit single-step time-marching discontinuous Galerkin methods with stage-dependent numerical flux parameters for a linear hyperbolic equation in one dimension*, J. Sci. Comput., 100 (2024). Paper No. 64.
[27] Q. Zhang and C.-W. Shu, *Error estimates to smooth solutions of Runge-Kutta discontinuous Galerkin methods for scalar conservation laws*, SIAM J. Numer. Anal., 42 (2004), pp. 641–666.
[28] ———, *Stability analysis and a priori error estimates of the third order explicit Runge-Kutta discontinuous Galerkin method for scalar conservation laws*, SIAM J. Numer. Anal., 48 (2010), pp. 1038–1063.
[29] X. Zhang and C.-W. Shu, *Positivity-preserving high order discontinuous Galerkin schemes for compressible Euler equations with source terms*, J. Comput. Phys., 230 (2011), pp. 1238–1248.